Biogeochemical model of nitrogen cycling in Ahe (French Polynesia), a South Pacific coral atoll with pearl farming

Claire Seceh, Christel Pinazo, Martine Rodier, Katixa Lajaunie-Salla, C. Mazoyer, Christian Grenz, R. Le Gendre

Biogeochemical model of nitrogen cycling in Ahe (French Polynesia), a South Pacific coral atoll with pearl farming

C. Seceh[1], C. Pinazo[1], M. Rodier[1], K. Lajaunie-Salla[1], C. Mazoyer[1], C. Grenz[1], R. Le Gendre[2]

1. Mediterranean Institute of Oceanography, Aix Marseille Univ., Université de Toulon, CNRS, IRD, MIO UM 110, 13288, Marseille, France

2. IFREMER, UMR9220 ENTROPIE, IRD, IFREMER, Université de la Réunion, CNRS, Université de Nouvelle-Calédonie, BP 32078, 98897 Nouméa, New-Caledonia

Corresponding author: claire.seceh@mio.osupytheas.fr

Abstract

A biogeochemical model (ECO3M-Atoll) was configured to simulate the lower food web in Ahe Atoll lagoon where phytoplankton is mostly nitrogen limited. Understanding the dynamics of phytoplankton – the main food source for oysters – is crucial for the management and the allocation of new pearl farming sites. After parametrizing the model with *in situ* observations, we tested different hypotheses about nitrogen cycling (benthic remineralization, atmospheric N fixation, etc.) and compared the results to a large observational dataset. Model results show that simulated (pico- and nano-) phytoplankton biomass and nitrogen concentrations are close to *in situ* data. The simulated biogeochemical processes (uptake and primary production) are also very similar to the observed values. In the model, primary production ranged from 1.00 to 2.00 mg C m^{-3} h^{-1} for pico- and 0.40 to 1.00 mg C m^{-3} h^{-1} for nanophytoplankton; mean N uptake was 2.02 µmol N m^{-3} h^{-1} for pico- and 1.25 µmol N m^{-3} h^{-1} for nanophytoplankton.

Keywords: Biogeochemical model; Ahe atoll; pearl farming; phytoplankton; nitrogen cycle

1. Introduction

After tourism, pearl farming represents the second largest source of income in French-Polynesia. The country dominated the market for black pearls during the 1980-90's. However, since the early 2000s, the sector is in crisis (Andréfouët et al., 2012), further exacerbated by the complexity of pearl farming. Pearl production depends on the life cycle of *Pinctada margaritifera* – the black-lip pearl oyster – and the success rate of farming is only about 30 % (about 300 sellable pearls per 1.000 grafted oysters) (Andréfouët et al., 2012).

In French Polynesia, pearl oysters are reared in fairly deep atoll lagoons. Atolls can be defined as productive micro-environments within an otherwise oligotrophic ocean. Indeed, atoll lagoons typically exhibit higher phytoplankton biomass and production compared to the

surrounding ocean (Charpy et al., 2012). Phytoplankton is the main food source for the oysters. During its two life stages (larvae and adult), *Pinctada margaritifera* feed on two different size classes of phytoplankton: while larvae consume mostly picophytoplankton (< 2 µm) adults prefer larger organisms such as nano- and microphytoplankton (> 2 and > 10 µm, respectively) (Pouvreau et al., 2000). Farmed oysters have to compete for phytoplankton with zooplankton and several filter feeders such as mollusks (clams or wild oysters).

In atoll lagoons, the availability of nutrients is one of the main drivers of phytoplankton growth. This bottom-up control depends on the atoll geomorphology (size, depth, and exchange with the open ocean). In deep or well flushed lagoons, primary production is typically more limited by nitrogen (N) than by phosphorus (P) (Dufour et al., 2001). The exact sources of N in these ecosystems is still unclear. Several studies have shown that remineralization sustains an important part of phytoplankton nitrogen uptake (Gaertner-Mazouni et al., 2012; Lacoste and Gaertner-Mazouni, 2016; Pagano et al., 2017). The most important sources of remineralized nitrogen are zooplankton, farmed oysters and associated epibionts (Lacoste and Gaertner-Mazouni, 2016), bacterial output and viral lysis (Shelford et al., 2012), coral and associated zooxanthella (Wild et al., 2004), and sediments (Gaertner-Mazouni et al., 2012). There are also several exogenous nitrogen sources including atmospheric N_2 fixation by diazotrophs (Charpy-Roubaud et al., 2001), geothermal endo-upwelling bringing up nutrients from the deep (Rougerie et al., 1992), rainfall, and of course anthropogenic inputs. Below, we will investigate some of these potential sources in more detail in order to assess their relative importance for Ahe Atoll.

To further improve our understanding of nutrient cycles in atoll lagoons, biogeochemical models (BGCMs) can provide a valuable framework. In tropical lagoons, BGCMs are often used to understand how interactions between compartments change when the lagoon is open or closed (Everett et al., 2007). Mongin and Baird (2014) used a BGCM to understand carbon calcification and the impact of climate change (heat stress) on Great Barrier Reef. In New Caledonia (Faure et al., 2010a,b; Fuchs et al., 2012, 2013; Hochard et al., 2010), modelling has been used to understand seasonal changes in local lagoons and the effects of strong events (El Niño and La Niña). However, only few studies have applied BGCMs to atolls. Niquil et al. (1998) developed an inverse model to describe the planktonic food web in the Takapoto Atoll (French Polynesia). Modelling was also used to understand the functioning of farmed lagoons in temperate environments. For example, they were used to understand biodeposition

due to farming (Weise et al., 2009), to manage clam farms (Marinov et al., 2007), or to investigate how farmed populations affect nutrient cycling (Cugier et al., 2010; Dowd, 2005).

In an effort to lend support to local pearl farmers and decision makers, this study adapted an existing BGCM (see below) and applied it to Ahe Atoll (French Polynesia), a semi-enclosed atoll environment with an extensive historical dataset useful for model validation (Bouvy et al., 2012; Charpy et al., 2012; Fournier et al., 2012; Lefebvre et al., 2012; Pagano et al., 2012; Thomas et al., 2010). A field campaign was conducted between November and December 2017 with the specific purpose to collect *in situ* observations that would allow the quantification (and thus parametrization) of the biogeochemical processes in the lagoon (Rodier et al., 2021). The sampling strategy was designed to be able to describe the biogeochemical state of the lagoon (*e.g.*, collecting phytoplankton biomass, dissolved organic and inorganic matter concentration) and to provide the necessary information to correctly parameterize the relevant dynamics in the BGCM (*e.g.*, primary production and nitrogen uptake rates). The model presented here is a 0-dimensional (variables vary only over time), deterministic BGCM that aims to capture the main biogeochemical processes taking place at the lower trophic levels. The aim of this paper is to provide a first glimpse of the parameter values that yield a satisfactory representation of the *in situ* ranges observed at Ahe Atoll.

The model is based on the ECO3M-Lagoon configuration (Faure et al., 2010a,b) and has been adapted for the Ahe Atoll. The simulation results provide a deeper understanding of the nitrogen cycling in the lagoon and were used to test the impact of pearl farming on the nitrogen cycle and phytoplankton biomass. Furthermore, the model was used to assess whether nitrogen input primarily results from benthic or exogenous sources. In addition, we tested the sensitivity of the new model configuration to different initial and light conditions and whether it can successfully reproduce the different biogeochemical regimes found in different parts of the lagoon. In the future, as part of the MANA (Management of Atolls) project, the model will be coupled with MARS3D, a hydrodynamic model (Lazure and Dumas, 2008), and with a dynamic energy budget (DEB) model developed by Thomas et al. (2016) and Sangare et al. (2019) to understand the physiology and spatial distribution of *P. margaritifera*. More precisely, the model will supply food inputs for studying the spawning of mature oyster and food inputs for development of larvae.

2. Materials and methods

2.1. Study site

Ahe Atoll is located in the north-western part of the Tuamotu Archipelago in French Polynesia, about 500 km north-east of Tahiti (

Fig. 1). Ahe is a semi-enclosed atoll with a lagoon that is connected to the open ocean by just one active pass on the north-western side of the atoll rim. Moreover, several *hoa* (shallow reef flat spillways) exist on the southern and north-western sides of the rim. The lagoon covers an area of 142 km^2 (main length = 23 km), has an average depth of 41 m (maximum 70 m), and a renewal time of about 250 days (Dumas et al., 2012). The climate is wet tropical with one rainy season from November to April. Maximum precipitation occurs in December and January. The air temperature varies only slightly over a year (25 – 29 °C). The wind regime is dominated by moderate trade winds blowing from East-South-East (60° to 160°) and with strong southerly winds in the austral winter (Dutheil et al., 2020). Our study period (November/December 2017) corresponds to the hot season at the beginning of the rainy period. Weather data indicated that while the rainy season had not yet started in November 2017, temperatures had already risen significantly since October 2017. During our field campaign, we only had one rain event (December 2, 2017) and a constant trade wind regime throughout.

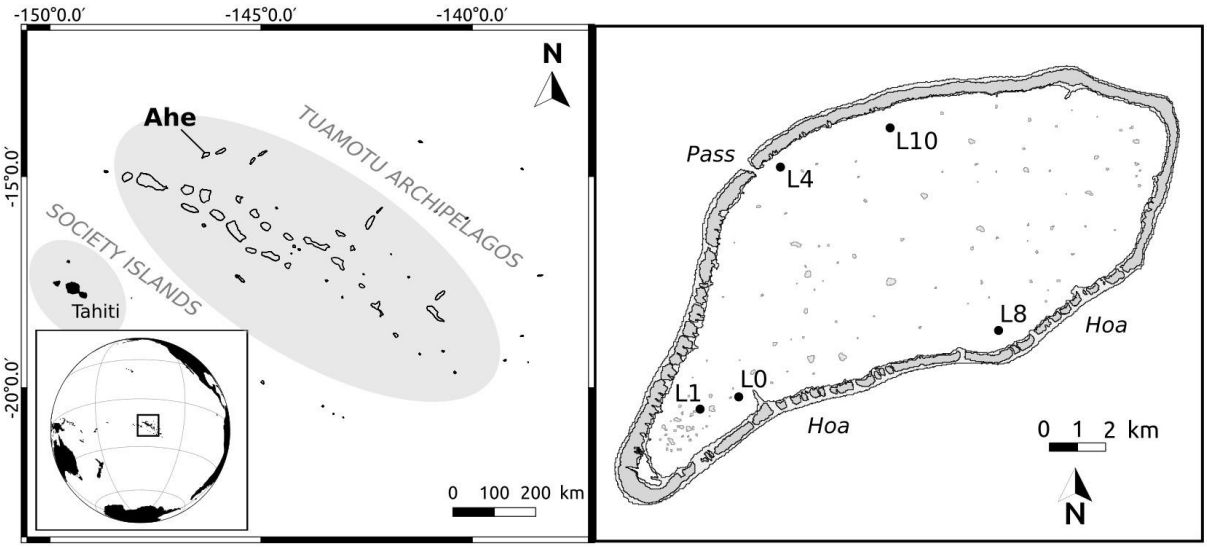

Fig. 1. Left: Location map of French Polynesia and Ahe Atoll. Right: Locations of sampling stations (black dots) and of the pass and hoa.

2.2. Dataset

For a multi-year model-data comparison, we used a large dataset consisting of data from campaigns that took place in the Ahe lagoon in 2007 and 2008 (Thomas et al., 2010), in 2010 (Charpy et al., 2012), in 2012 and 2013 (Pagano et al., 2017), and in 2017 (Sangare et al., in prep.). In order to implement and calibrate some of the key biogeochemical processes in the model, we used data obtained at five stations in the lagoon (L0, L1, L4, L8, and L10 in **Fig. 1**) during a single field campaign (AHE2017) that took place between November 27 and December 07, 2017. More details about the sampling and analysis can be found in Rodier et al. (2021).

At each station, vertical profiles of temperature, salinity, photosynthetically active radiation (PAR), and dissolved oxygen concentration were recorded with a Seabird 19+ CTD profiler of which we only used the values from 5 m. At L0, the CTD was also deployed in mooring mode at a fixed depth of 5 m between Nov 29, 14:00h and Dec 01, 17:00h (total of 51 h) and between Dec 02, 16:00h and Dec 04, 08:00h (total of 40 h). This time series data was used to parameterize the daily light availability.

Inorganic nutrients (NH_4^+, NO_2^- + NO_3^- = NOx, PO_4^-) and dissolved and particulate organic matter (C, N, P) were sampled. < 2 µm, > 2 µm, and > 10 µm Chla size classes representing pico-, nano- and microphytoplankton biomass proxies, respectively, were also collected. For reasons of simplicity, we grouped nano- and microphytoplankton together and will refer to them collectively as nanophytoplankton throughout this manuscript. Microphytoplankton are less common than nanophytoplankton in the Ahe lagoon, accounting for less than 10 % of the total Chla (Charpy and Charpy-Roubaud, 1990).

To improve the model parameterization, we also measured several biogeochemical pelagic and benthic fluxes that are not usually measured.

Carbon fixation (primary production) and nitrate and ammonium uptake rates of pico- and nanophytoplankton were measured at each station ($^{13}C/^{15}N$ method). At L0, we also obtained vertical profiles of primary production from the surface to a depth of 40m, at 5m intervals. The resulting P/I curve was used to calibrate the relationship between solar irradiance and photosynthesis in the model. Daily primary production was calculated from carbon fixation and a photoperiod of 11.5h.

Finally, benthic flux chambers were deployed at each station to quantify nutrients (NH_4,

NO_x, $Si(OH)_4$, PO_4) and oxygen fluxes at the sediment-water interface. Two different kinds of chambers were used: one opaque chamber to simulate nighttime and a transparent chamber to expose the sediments to the ambient light regime. More details can be found in Grenz et al. (this issue).

2.3. Biogeochemical model configuration: ECO3M-Atoll

ECO3M-Atoll was adapted from the ECO3M-Lagoon configuration used by Faure et al. (2010a, b) and by Fuchs et al. (2013, 2012) for the south-western lagoon of New Caledonia (**Fig. 2**). They are based on the ECO3M platform developed by Baklouti et al. (2006a,b). One of the main improvements over the ECO3M-Lagoon configuration, is that ECO3M-Atoll uses two phytoplankton compartments for pico- and nanophytoplankton, respectively. While the model has a typical NPZD (nutrients, phytoplankton, zooplankton, and detritus) structure, zooplankton is parameterized as a "theoretical" population, i.e., it has no specific state variable but all physiological functions and processes are described implicitly. Mass conservation is achieved through a function that parameterizes predation by higher trophic levels.

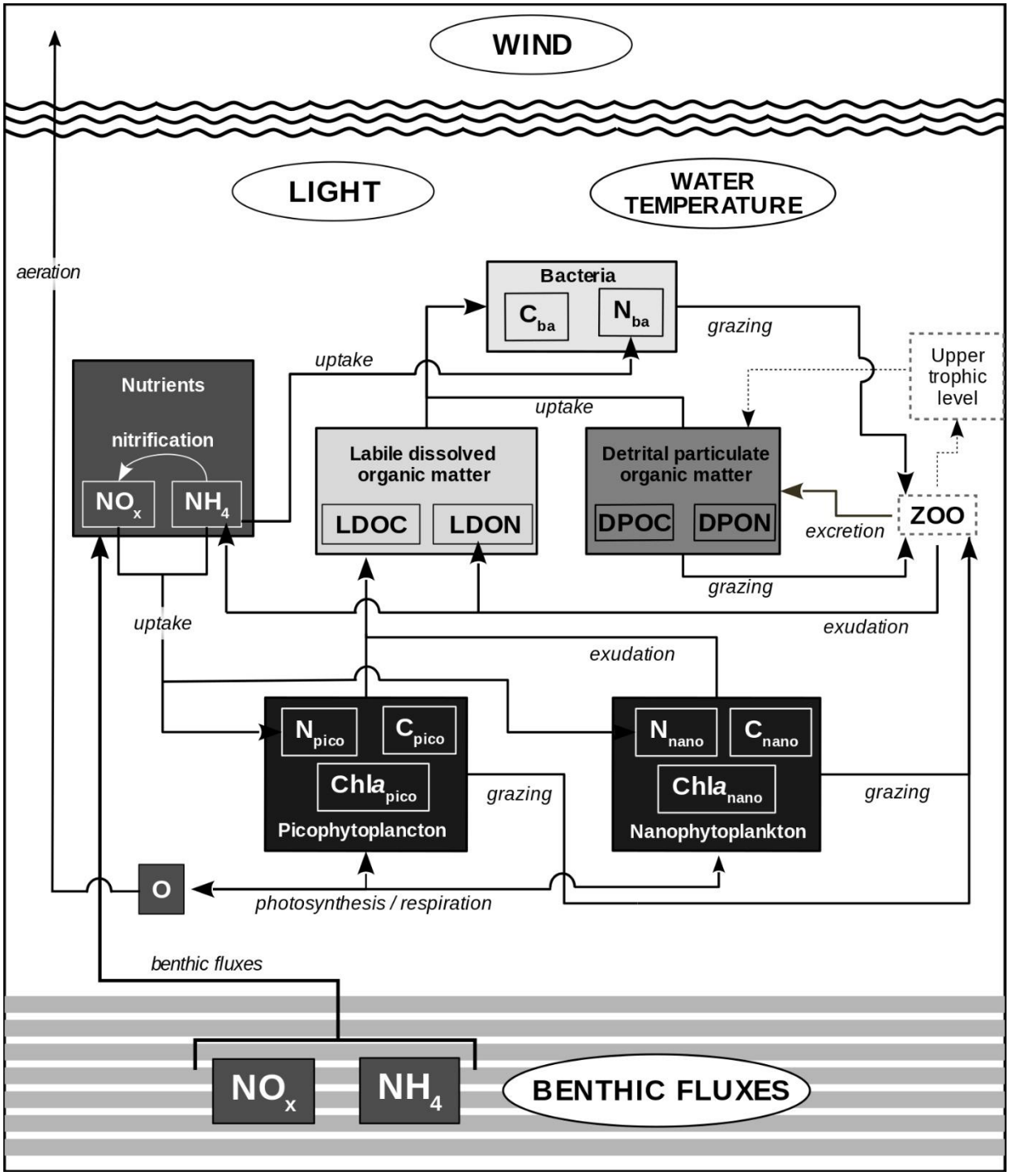

Fig. 2. Schematic diagram of the biogeochemical cycles represented in the ECO3M-Atoll model showing all state variables, processes, and forcings.

The model describes both the carbon and nitrogen cycles and consists of six compartments that use either carbon or nitrogen units: picophytoplankton (pico-), nanophytoplankton (nano-), bacteria, detritic particulate organic matter (DPOM), and labile dissolved organic matter (LDOM). At Ahe, phytoplankton are not limited by phosphorus (Charpy et al., 2012). The DOM compartment contains ammonium (NH_4), nitrate + nitrite (NO_x), and dissolved oxygen (O_2). In total there are 15 state variables (**Table 1**), and even chlorophyll *a*, which is a diagnostic variable, is also calculated from the phytoplankton's internal N/C ratio $Q_C^N phyto$ (Faure et al., 2006, 2010a; Smith and Tett, 2000) (see Appendix A). Moreover, this internal N/C ratio varies between prescribed phytoplankton-specific upper and lower bounds and is recalculated at each time step. This ratio contains information about the nutritional state of the cells when compared to the Redfield ratio (Redfield et al., 1963). This nutritional state is taken into account to calculate the growth and nutrient uptake rates (Tett, 1987). The same framework is used to express bacterial processes (Thingstad, 1987).

Table 1. State variables used in the ECO3M-Atoll model (except Chla which is a diagnostic variable).

Variables	Definitions	Units
C_{pico}	Picophytoplankton carbon	µmol L^{-1}
C_{nano}	Nanophytoplankton carbon	µmol L^{-1}
N_{pico}	Picophytoplankton nitrogen	µmol L^{-1}
N_{nano}	Nanophytoplankton nitrogen	µmol L^{-1}
Chla_{pico}	Picophytoplankton chlorophyll *a*	µg Chl*a* L^{-1}
Chla_{nano}	Nanophytoplankton chlorophyll *a*	µg Chl*a* L^{-1}
C_{ba}	Bacteria carbon	µmol L^{-1}
N_{ba}	Bacteria nitrogen	µmol L^{-1}
DPOC	Detrital particulate organic carbon	µmol L^{-1}
DPON	Detrital particulate organic nitrogen	µmol L^{-1}
LDOC	Labile dissolved organic carbon	µmol L^{-1}
LDON	Labile dissolved organic nitrogen	µmol L^{-1}
NH_4	Ammonium	µmol L^{-1}
NO_x	Nitrates	µmol L^{-1}

O	Oxygen	µmol L^{-1}

As the phytoplankton variables were split into two different size classes (compartments), new equations were added and others from the original ECO3M-Lagoon configuration had to be updated. The parameter values were chosen based on the *in situ* data collected during the AHE2017 field campaign (Rodier et al., 2021) (**Table 2**).

The initial slope of the P/I curve (**Fig. 3.A)** was used to determine the Chl-specific light absorption coefficient (α_{Chla}, **Table 2**). This coefficient is used to calculate pico- and nanophytoplankton growth (Eqs. 1-3). To simplify, we use the subscript "phyto" to denote both pico- and nanophytoplankton (see Appendix B).

$$P^{C}_{phyto} = \mu_{max}(T)_{phyto} \cdot \left[1 - \exp\left(\frac{-\alpha_{Chla} \cdot PAR \cdot Q_C^{Chla}}{\mu_{max}(T)_{phyto}}\right)\right] \quad (1)$$

$$\mu_{max}(T)_{phyto} = a_{phyto} \cdot \exp(b_{phyto} T) \cdot Q_{phyto} \quad (2)$$

$$Q_{phyto} = \frac{Q_C^N phyto - \min Q_C^N phyto}{\max Q_C^N phyto - \min Q_C^N phyto} \quad (3)$$

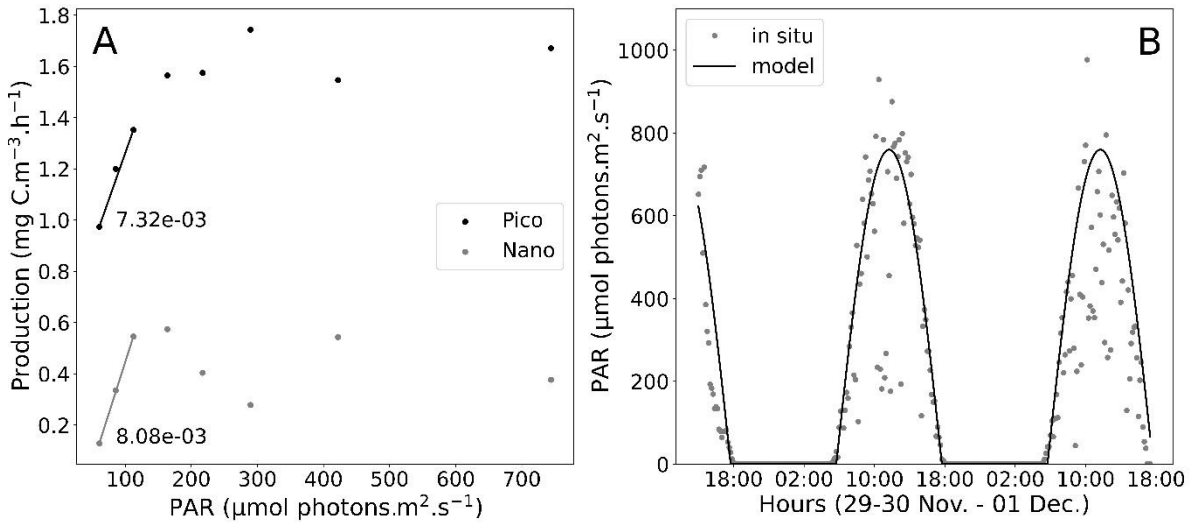

Fig. 3. A: Production/Irradiance curve of pico- (black) ad nano- (grey). **B**: PAR measurement (grey dots) and light function (black line).

Table 2. Parameters values for pico- and nanophytoplankton used during the calibration simulation at L0.

Parameters (units)	Pico-	Nano-	References

αChla (mg C. $m^{-1}.h^{-1}$. (µmol photons $.s^{-1})^{-1}$)	7.32×10^{-3}	8.08×10^{-3}	**Fig. 3.A**
max V_{NH4} (µmol N . m^{-3} . h^{-1})	22	11	Rodier pers. comm.
max V_{NOx} (µmol N . m^{-3} . h^{-1})	6	4	
µmax (d^{-1})	0.70	0.34	
g (d^{-1})	1.89	1.47	Projet 9ème FED Professionnalisation et perennisation de la perliculture, 2010
K_{NH4} (mmol N . m^{-3})	0.05	0.30	Assumed
K_{NOx} (mmol N . m^{-3})	0.60	1.12	

All our simulations were made in 0D and over a period of 300 days to reach a steady state, representative of a 5 m depth water cell. The temporal evolution of biogeochemical processes or variable concentrations has the same shape (Supplementary Figure 1S). The curve shows a spin-up period lasting 25 days. From the beginning of the simulation, the modeled phytoplankton are nutrient limited. Then, after about 50 days, the model tends to reach a steady state and is fully limited by nutrients. Results shown below correspond to daytime values (as all *in situ* data was measured during daytime) after 200 days once the simulation had become stable .

The model was forced using realistic average temperatures, wind velocities , and light intensities in order to reproduce the ecosystem functioning at 3m depth. All stations used the same constant temperature and wind speeds of 28.4 °C and 5.4 m s^{-1}, respectively, corresponding to the mean *in situ* values during the AHE2017 campaign. Wind was used only to drive oxygen aeration and light was prescribed based on a day/night cycle using actual PAR measurements at L0 (**Fig. 3.B**):

$$PAR = max\left(0, PAR_{max} \times sin\left(\pi \times \frac{t}{12}\right)\right) (4)$$

where PAR_{max} is the maximum value of PAR (in µmol photons s^{-1}) at noon and t is time (in hours).

Different metrics are used for the statistical model-data comparison. The mean absolute error (MAE), the root mean square error (RMSE), the percentage model bias (PB), and the Willmott index (d1) (Willmott, 1982) are calculated using:

$$MAE = \frac{\sum_{i=1}^{n}|M_i - D_i|}{n} \quad (5)$$

$$RMSE = \sqrt{\frac{\sum_{i=1}^{n}(M_i - D_i)^2}{n}} \quad (6)$$

$$PB(\%) = \frac{\sum_{i=1}^{n}(D_i - M_i)}{\sum_{i=1}^{n} D_i} \times 100 \quad (7)$$

$$d1 = 1 - \frac{\sum_{i=1}^{n}(M_i - D_i)^2}{\sum_{i=1}^{n}\left((M_i - \overline{D}) + (D_i - \overline{D})\right)^2} \quad (8)$$

2.4. Simulation strategy

2.4.1. Sensitivity to environmental forcing

Simulations to test model sensitivity to environmental forcing and parameters were performed at station L0 (**Table 3**) where the continuous PAR measurements were performed. To assess the model sensitivity to external forcing, the light and temperature ranges were chosen to be representative of the typical values encountered in Ahe atoll. The light range is based on PARmax (see Section 2.2). The temperature range was chosen based on a one-year *in situ* dataset (Sangare, pers. comm.).

2.4.2. Sensitivity to model parameters

The sensitivity analysis was performed using the index described by Chapelle et al., (2000)*:*

$$IS\% = \left(\frac{100}{p}\right) \cdot \frac{1}{N} \sum_{i=1}^{N} \frac{|X_i - X_i^{raw}|}{X_i^{raw}} \quad (9)$$

where p is the percentage of parameter change (± 10 % in this study), N = 3600 (only the last 150 days are taken into account with hourly results), X_i is the variable value at time t after the parameter change, X_i^{raw} is the variable value at time t in the control simulation. IS% is used to identify the most sensitive parameters (*i.e.,* parameters whose variation causes the strongest deviation of state variables from the reference simulation).

Table 3. Initial conditions for the five Ahe stations.

	L0	L1	L4	L8	L10
C_{pico} *(µmol.L^{-1})*	0.709	0.710	0.347	0.276	0.379
N_{pico} *(µmol.L^{-1})*	0.029	0.108	0.053	0.042	0.058
$Chla_{pico}$ *(µg Chla.L^{-1})*	0.259	0.238	0.116	0.093	0.127
C_{nano} *(µmol.L^{-1})*	0.187	0.196	0.066	0.049	0.066
N_{nano} *(µmol.L^{-1})*	0.029	0.030	0.010	0.007	0.010
$Chla_{nano}$ *(µg Chla.L^{-1})*	0.069	0.081	0.027	0.020	0.027
C_{ba} *(µmol.L^{-1})*	0.83	0.83	0.83	0.83	0.83
N_{ba} *(µmol.L^{-1})*	0.14	0.14	0.14	0.14	0.14
DPOC *(µmol.L^{-1})*	3.98	16.67	2.50	12.50	12.50
DPON *(µmol.L^{-1})*	1.25	2.143	0.71	1.79	1.43
LDOC *(µmol.L^{-1})*	7.50	10.80	9.57	8.76	8.76
LDON *(µmol.L^{-1})*	2.40	2.65	2.18	1.95	2.16
NH_4 *(µmol.L^{-1})*	0.012	0.013	0.028	0.012	0.025
NO_x *(µmol.L^{-1})*	0.187	0.085	0.073	0.058	0.091
O *(µmol.L^{-1})*	190	186.5	186.8	181.9	184.1

After this initial sensitivity analyses, two types of simulations were run: a reference simulation (control) – testing the sensitivity to initial conditions – and simulations to test various hypotheses about N inputs and grazing. The initial conditions of state variables were set according to *in situ* the values at each station (**Table 3**).

2.4.3. Sensitivity to initial conditions at the five stations

Reference simulations (named S0) were run at all stations (L0 to L10) with the same parametrization but different initial conditions. These simulations allowed us to compare modelled fluxes (nutrients uptake rates and primary production), final nutrient concentrations,

and phytoplankton biomass to *in situ* values at each station.

Four other simulations testing the process hypotheses were performed at all stations to study the model response to changes in grazing, benthic fluxes, N fixation, and NO_x inputs. The influence of two different kinds of nitrogen sources were tested.

2.4.4. Sensitivity to grazing mortality

Lacoste and Gaertner-Mazouni (2016) showed that nitrogen remineralization due to the grazing by oysters (and associated epibiont filter-feeders) was stronger than nitrogen remineralization in the sediment. Therefore, we ran several grazing simulations (S1.1, S1.2, S1.3). Grazing rates were taken from the report of Projet 9ème FED Professionnalisation et perennisation de la perliculture (2010). In S1.1, the grazing value for nanophytoplankton was increased from 1.45 to 2.50 d^{-1} to account for grazing by mesoplankton, oysters, and other higher predators. In S1.2, picoplankton grazing was increased from 1.70 to 1.85 d^{-1} to account for grazing by nano- and mesoplankton. In S1.3, the grazing rate in both phytoplankton compartments was increased.

2.4.5. Sensitivity to N-cycle components

Other N-cycle components were tested. In simulation S2, we added *in situ* benthic fluxes obtained in 2017 using benthic chambers. Benthic nitrate and ammonium fluxes were implemented as follows: the fluxes measured in dark chambers were used during night-time and those measured in transparent chambers during the day were used during daytime (**Table 4**). Moreover, as demonstrated by Charpy-Roubaud et al. (2001) at Tikehau Atoll, benthic nitrogen fixation may take place in the sediment. Therefore, in simulation S3 simulation we applied a NH_4 influx of 0.18 µmol L^{-1} h^{-1}. In simulation S4, an exogenous input of 0.36 µmol L^{-1} h^{-1} of NO_x was used. We measured high NO_x values in rainwater (49 µmol L^{-1}) and in the ground water below a *motu* (a coral sand island on the reef crown of an atoll) north of Ahe Atoll (38 µmol L^{-1}).

Table 4. Benthic fluxes in the model in µmol m^{-2} h^{-1}. Positive values represent fluxes from the sediment to the water column and negative values represent fluxes from the water column to the sediment.

	NH4		NOx	
	Day	Night	Day	Night

L1	+8	+2	+63	-90
L4	+1	+0.3	+0.8	-12
L8	+7	+5	+85	-125
L10	+1.5	-3.4	+5.8	-25

3. Results

Three types of sensitivity analyses were performed on the control simulation: sensitivity to forcing conditions, to initial conditions, and to the choice of parameter values.

3.1. Sensitivity to environmental forcing

PARmax and the water temperature were increased in 10 steps from 100 to 1300 µmol photons m^{-2} s^{-1} and 23 to 31 °C, respectively. We then compared the final pico- and nano-biomasses obtained for these different forcing levels (**Fig. 4**).

Pico- is more sensitive to changes in environmental forcing than nano-. Indeed, pico- varies between 0 and 0.2 µg Chla.L^{-1}, while nano- varies between 0 and 0.125 µg Chla L^{-1}. Moreover, below about 250 to 400 µmol photons m^2 s^{-1}, the impact of temperature changes are rather small on phytoplankton biomass, resulting in a pico- biomass of 0.0 and 0.10 and nano- biomass of 0 and 0.075 µg Chla L^{-1} for temperatures of 31°C and 25°C, respectively. For higher light intensities, primary production is no longer light-limited and becomes more sensitive to temperature. For example, at 700 µmol photons m^2 s^{-1}, the pico- biomass is 1.6 times higher and the nano- biomass increased by a factor 2.

For the light and temperature ranges observed during the AHE2017 campaign, *i.e.*, temperatures between 28.3 and 29.5°C and PAR between 550 and 1200 µmol photons m^2 s^{-1}, the model predicts only very small changes in phytoplankton biomass (white box in **Fig. 4**).

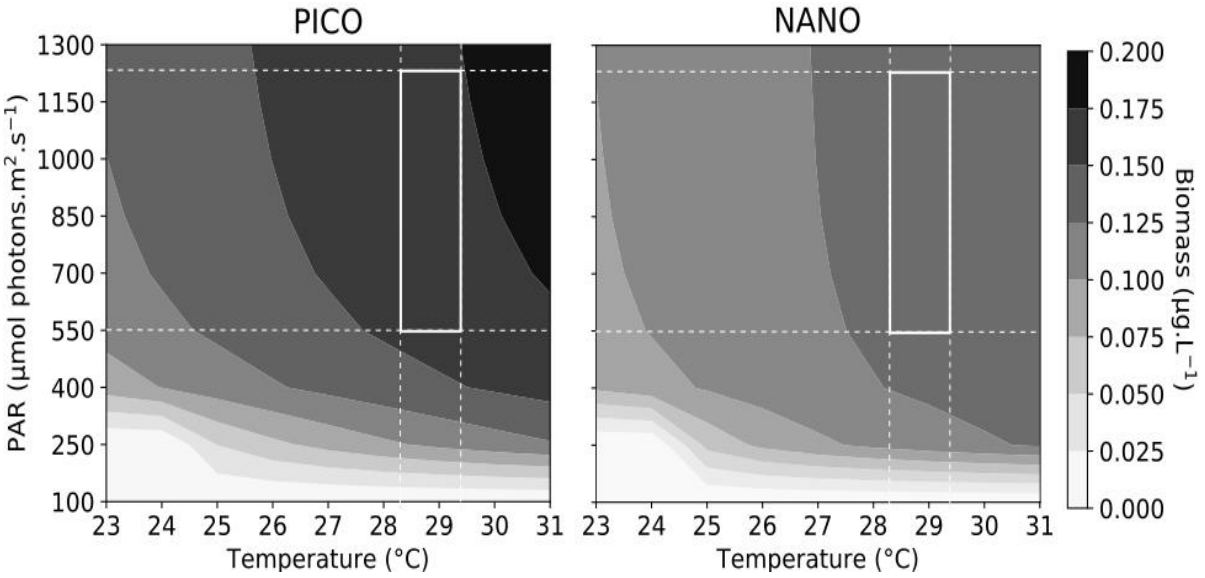

Fig. 4. Influence of temperature and maximum daily PAR on pico- (left) and nano- (right) biomass (µg Chla L^{-1}). The white box represents the *in situ* light and temperature ranges encountered during the AHE2017 campaign.

3.2. Sensitivity to model parameters

Indices of sensitivity (IS) for phytoplankton chlorophyll a, nutrients, and dissolved and particulate organic nitrogen are presented for a ± 10 % variation in parameter values (**Fig. *5***). The fractions of dissolved organic carbon (d_C) and nitrogen (d_N) assimilated by zooplankton were found to be the most sensitive parameters and influence all the state variables shown in **Fig. 5**. These parameters represent the ratio of the dissolved over the particulate pool, once assimilated by zooplankton and upper trophic levels. Increasing d_C by 10 % led to an IS of 31 % for NO_x and 17 % for LDON. A 10 % decrease in d_N yielded an IS of 37 % for NO_x and 19% for LDON. Grazing parameters (g_{pico}, g_{nano}) are also sensitive and mainly impact the phytoplankton and nutrients. IS for pico- is about 1.36 and 1.10 % for -10 and +10 % changes in g_{pico}, respectively. The same variations in g_{nano} produce IS values for nano- of 1.28 and 1.07 %, respectively. The same variations in grazing rates yield a maximum IS for NH_4 of 2.02 %. Also, µmax mainly impacts nutrients and phytoplankton as it controls phytoplankton biomass production and, in turn, the nutrient concentrations through the microbial loop. Unsurprisingly, maxV, *i.e.*, the maximum nutrient uptake rate (NH_4 and NO_x) by phytoplankton, affects nutrient concentrations.

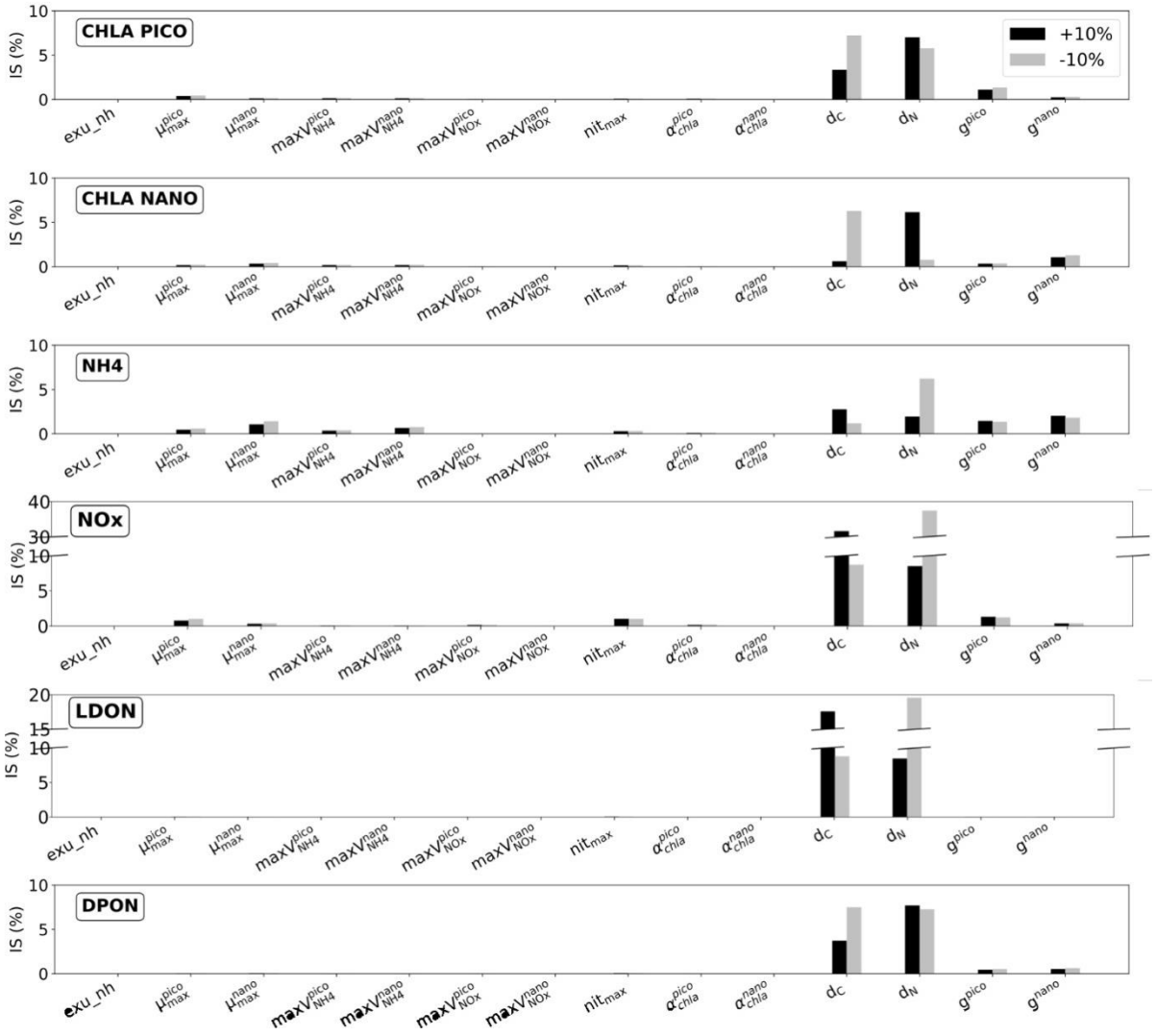

Fig. 5. Mean IS% index calculated for Chlorophyll a (pico- and nano-), nutrients (NH_4 and NO_x), and dissolved and particulate organic nitrogen (LDON and DPON) concentration.

3.3. Sensitivity to initial conditions at all five stations

The reference simulation (S0) was performed to compare modelled to *in situ* data. More specifically, we focused on the maximum NH_4 and NO_x uptake rates and primary production (occurring during the model spin-up). While phytoplankton did not seem to be nutrient limited during the field experiments (Rodier et al., 2021), the model was set up with nutrient limitation. Moreover, while uptake rates in the field were measured for NO_3, the model uses uptake rates for NO_x which seemed justified since NO_x is essentially represented by NO_3 in Ahe lagoon (Charpy et al., 2012). Results of primary production (**Fig. 6.A**) show a clear spatial pattern with maxima of about 2 mg C m^{-3} h^{-1} for pico- and 1 mg C m^{-3} h^{-1} for nano- at Station L1, which seems to be about 2 to 3 times more productive than other stations. At all

stations, nano- contributed between 25 and 40% to the total primary production, with a lagoon-wide average of 32%. Moreover, the three southern stations (L0, L1 and L8) seem to show a higher proportion of PP by nano- compared to the two northern stations.

NH_4 and NO_x uptake rates from the model and *in situ* observations cannot be compared quantitatively because of the difference between nutrient limitation during the experiments and in the model. . However, we can compare the ratios between pico- and nano- and between NH_4 and NO_x uptake rates at different stations. Everywhere, uptake of NH_4 was greater than of NO_x (**Fig. 6.B**.). Moreover, uptake rates were greater at L1 and lower at L4. The NH_4 uptake by pico- represented more than 50% of the total NH_4 uptake, except at L1 and L8. At all stations except L1, NO_x uptake appears lower than NH_4 uptake. The NO_x uptake by pico- at L1 and L8 represent 70% of the total and more than 80% at L0, L4, and L10.

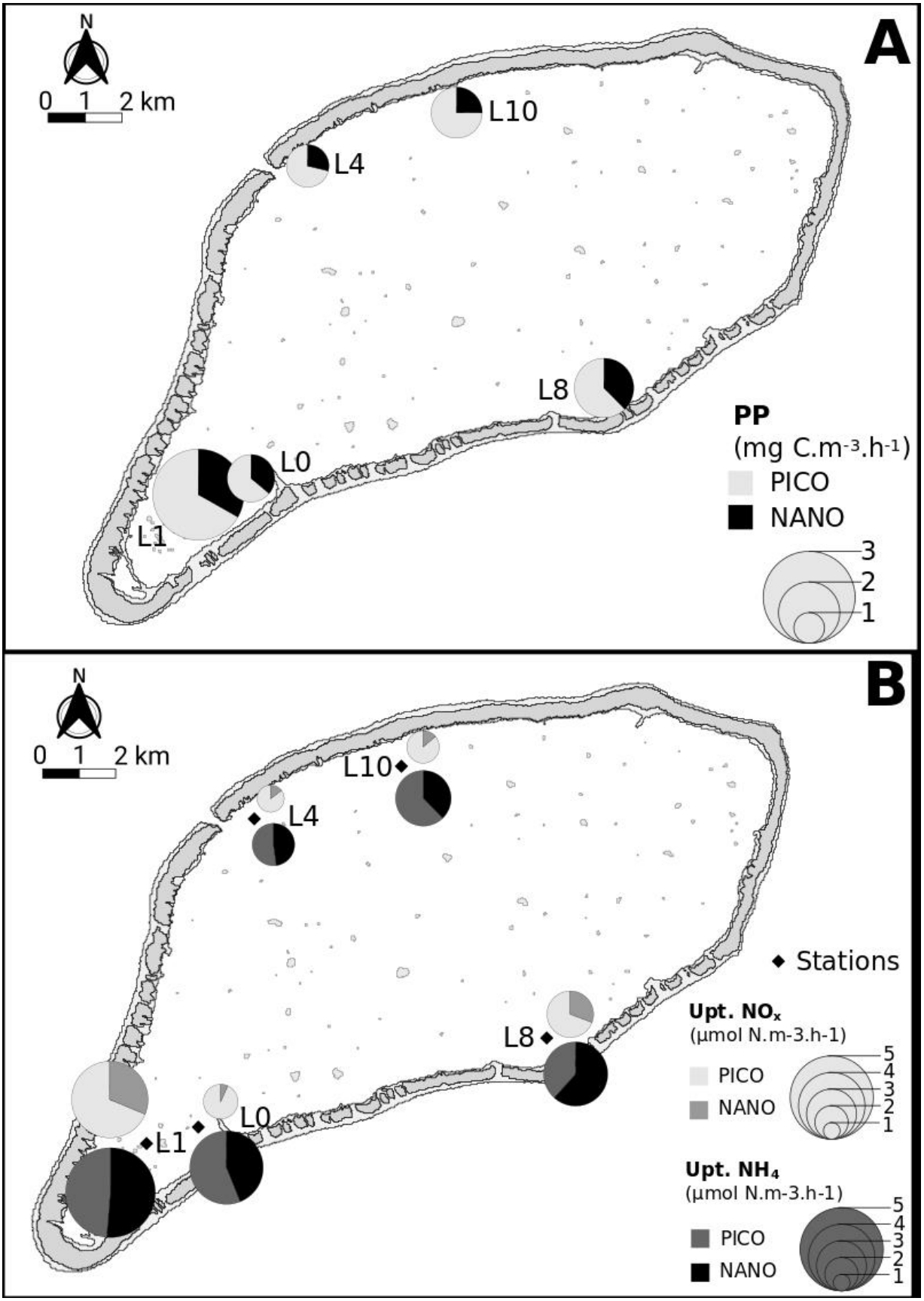

Fig. 6. Maps of modeled biogeochemical fluxes at all 5 stations. **A**: Primary production (PP) by pico- and nano-. **B**: Uptake rates of NH_4 and NO_x by pico- and nano-.

From among the different statistical metrics used, MAE and RMSE show best results for pico-, NH_4, and NO_x (**Table 5**). Bias can be considered poor when its value is above 40 % (Maréchal, 2004). Pico- and NOD have the lowest bias. Uptake rates of NH_4 and NO_x show a good result for d1 with significant values for PP, pico-, nano-, NH_4 and NO_x.

Table 5. Statistical analyses comparing observations with model results of the S0 simulation. MAE = Mean Absolute Error, RMSE = Root-Mean-Square Error, d1 = Willmott index (1982). Note that the row "Uptake NH_4 and NO_3" represents the ratio between the pico- and nano- uptake. * Significant values of d1 (> 0.70).

	MAE	RMSE	Bias (%)	d1
PP	0.40	0.94	61.70	0.77*
Uptake NH_4 NO_3	0.27	0.12	43.02	0.10
Pico-	0.028	0.004	12.22	0.66
Nano-	0.972	0.258	317.82	0.14
NH_4	0.036	0.070	74.05	0.48
NO_x	0.091	0.171	49.26	0.21
NOD	2.715	0.920	22.52	0.26

A graphical comparison is shown in **Fig. 7** and **Fig. 8**.

3.4. Sensitivity to grazing

At each station and for each grazing scenario, the pico- biomass was lower than in S0 even if the nano- grazing rate was increased (**Fig. 7**). In contrast, the nano- biomass was lower when the nano- or both the pico- and nano- grazing rates were increased (S1.3). At all stations, the S1 and S0 nano- biomasses are nearly identical. At L1 and L4, the S1.1 and S1.3 nano- biomasses we are very similar. Overall, the simulated pico- biomass appears to be closer to *in situ* values at L4 and L8. Comparing between different simulations, the nano- biomass appears closer to *in situ* values in S1.1 and S1.3. In all grazing simulations, NH_4 and NO_x concentrations were higher than in S0, increasing from about 0.012 to 0.035 µmol L^{-1} for NH_4 and 0.10 to 0.18 µmol L^{-1} for NO_x, when the grazing rates are increased. This increase is more pronounced when just the nano- or both the pico- + nano- grazing rates are increased. In these three simulations, the nutrient concentrations were closer to *in situ* values at L1, L4, and

L8 for NH_4 and at L4, L8, and L10 for NO_x. Finally, LDON concentrations did not affect these grazing simulations.

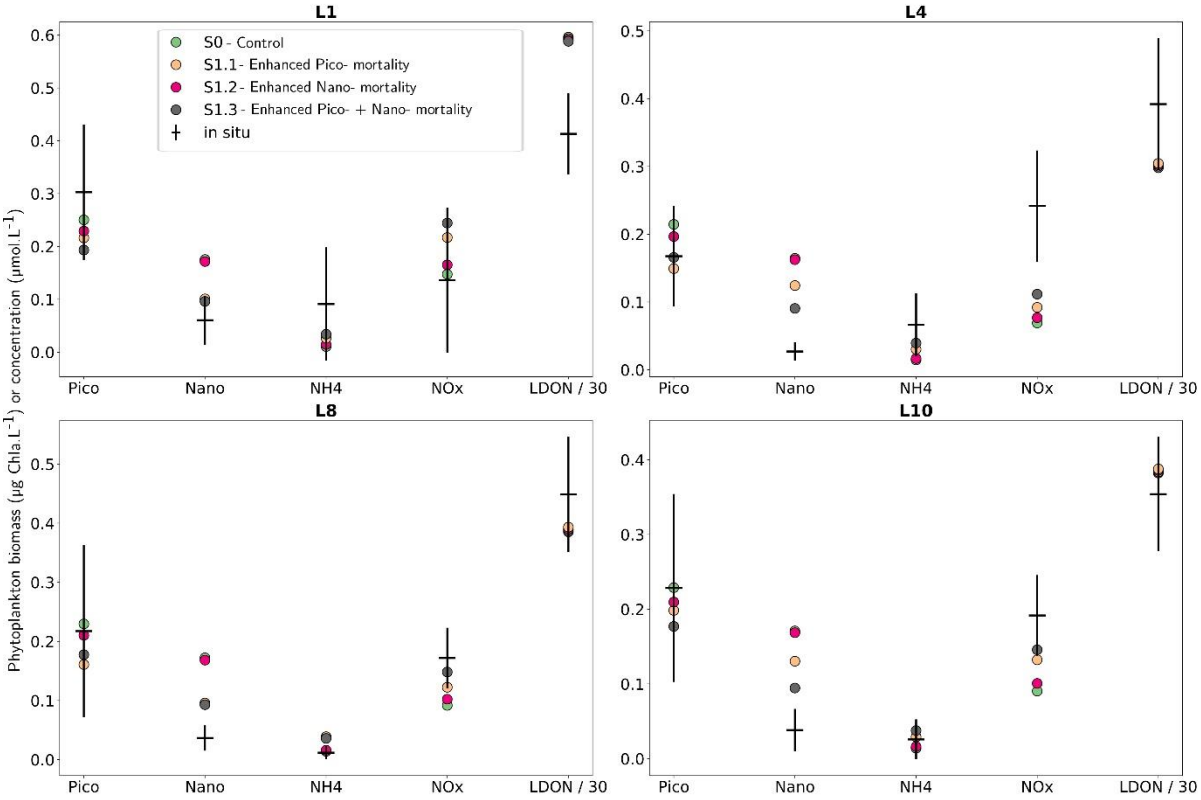

Fig. 7. Comparison between *in situ* data and the SO and S1.1-3 model outputs at four stations. Reminder: S0 – control, S1.1 – higher pico- grazing, S1.2 – higher nano- grazing, and S1.3 – higher pico- + nano- grazing. Black vertical bars represent one standard deviation and black horizontal bars represent *in situ* means. Note that LDON values have been divided by 30 to fit onto the scale of this figure.

3.5. Sensitivity to N-cycle components

Benthic fluxes measured at the sediment - water interface show some differences between NH_4 and NO_x fluxes (Grenz et al., this issue). NH_4 fluxes were always positive (*i.e.*, from sediment to water column) except at L10 where they were negative during the day. In contrast, NO_x fluxes were always positive during nighttime and always negative during daytime. Moreover, NH_4 fluxes were lower than NO_x fluxes (**Table 4**). These benthic fluxes varied between stations with higher values observed at L1 and L8 (Grenz et al., this issue). In the S2 simulation (benthic fluxes simulation), NO_x concentrations at L1 and L10 decreased significantly (by about 0.1 µmol L^{-1}), while at other stations this decrease was less pronounced (about 0.05 µmol L^{-1}). Modeled LDON was also lower at all stations. Concerning

NH_4, no variation of concentrations is observed. Benthic fluxes reduced ambient NO_x concentrations. These NO_x concentrations are lower than *in situ* data at all stations, except at L1 where they are within the standard deviation. Overall, the modeled phytoplankton biomass was lower at each station, with the simulated nano- biomass closer to *in situ* values at all stations except L4.

In the nitrogen fixation simulation (S3), all variables were higher than *in situ* values. N fixation had no effect on NH_4 concentration but led to high NO_x concentrations at L4, L8, and L10. Moreover, the simulation results were improved with regard to the pico- biomass at L1.

Compared to S3, the S4 simulation, which considers anthropogenic inputs of NO_x, led to an even higher increase in concentrations at all stations, except for nano-. Moreover, the S4 pico-biomass was closer to *in situ* data at L1 and NO_x at L4.

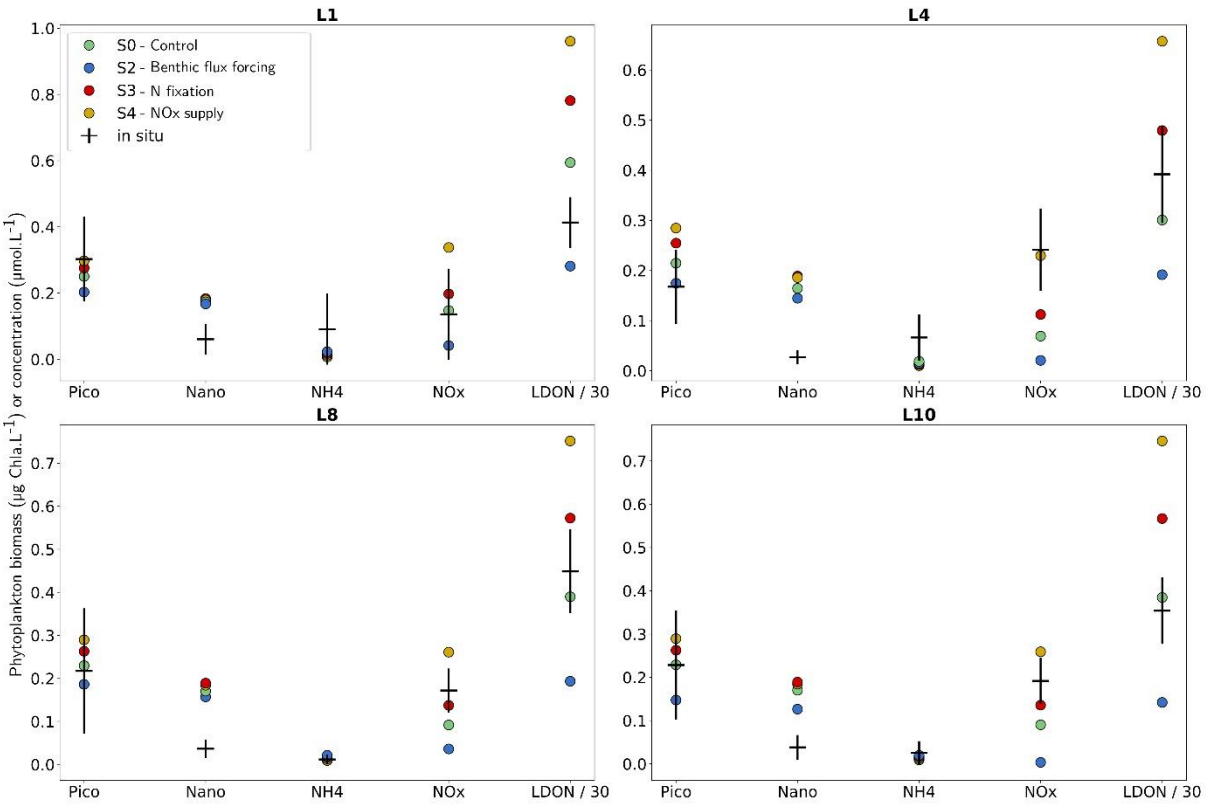

Fig. 8. Comparison between *in situ* data and model outputs. Reminder: S0 – Control, S2 – benthic flux forcing, S3 – N fixation, and S4 – NO_x supply. Black vertical bars represent one standard deviation and black horizontal bars represent *in situ* means. Note that LDON values have been divided by 30 to fit the scale of this figure.

4. Discussion and conclusion

4.1. Sensitivity analysis

The sensitivity analysis on forcing conditions suggested us to set the same light and temperature on all stations. We observed no significant changes in the pico- or nano-biomasses when varying the forcing conditions within the ranges observed during the AHE2017 field campaign. We therefore applied the same constant environmental forcing (water temperature of 28.5°C and PAR_{max} of 800 µmol photons m^{-2} s^{-1}) across the model domain. Moreover, this analysis confirms that the model conveys the lack of photo-inhibition measured in the Ahe lagoon (Lefebvre et al., 2012). This is partly due to the shape of the primary production equation and, more specifically, how it accounts for light limitation (see Appendix A.1.2). The lagoon typically exhibits higher temperatures in its south-western part (Dumas et al., 2012; Rodier et al., 2021). While this higher temperature may affect phytoplankton communities and the overall biogeochemistry, it is not taken into account by our present model. In the future, by implementing different PAR and temperature values at different locations, the model may be able to account better for these spatial heterogeneities.

The sensitivity analysis allowed us to understand the behavior of the new model configuration and identify differences compared to the Caledonian configuration. Compared to the sensitivity analysis of the ECO3M Lagoon configuration in Faure et al. (2010a), the ECO3M-Atoll configuration appears less sensitive. The model appeared most sensitive to changes in the fraction of dissolved organic matter (carbon and nitrogen) assimilated by zooplankton (parameters d_C and d_N, respectively), the grazing rate (g), and the maximum phytoplankton growth rate (µmax). d_C affects carbon assimilation, but also nitrogen (NH_4, NO_x, LDON and DPON). This can be explained by the fact that the model allows a variable stoichiometry. Nutrient uptake is controlled by the external nutrient concentrations and an internal quota function based on the N/C ratio. Therefore, when d_C changes, the phytoplankton carbon varies and N/C is modified because of respiration which is not controlled by the quota function but set to a constant value (R_{phyto}). This modulates the uptake rate and impacts NH_4 concentration. While this phenomenon may also exist in the ECO3M-Lagoon configuration, it may be amplified in the present configuration which has two phytoplankton compartments instead of only one. Moreover, as in the ECO3M-Lagoon configuration, nutrients were more sensitive to parameter changes than phytoplankton biomass. In summary, our analysis confirmed that that changes in grazing mostly affect phytoplankton and ammonium as grazing not only has a direct impact on the amount of

phytoplankton grazed but also indirectly affects NH_4 via the remineralization through the microbial loop.

4.2. Biogeochemical fluxes in the water column

The model parameters were based on specific *in situ* measurements of nutrients and phytoplankton concentrations as well as biogeochemical processes (Rodier et al., 2021). Some of the model results presented in Section **3.3**were close to *in situ* data. The model predicted the share of nano- in the total primary production in the lagoon to be 32 % while *in situ* data suggests a contribution of 25 ± 12 %. There was a clear difference between the northern and southern parts of the lagoon: while nano- contributes only about 25 % of total primary production at the northern L4 and L10 stations, in the south at L0, L1, and L8 it is of the order of 40 % (**Fig. 6A**). In the *in situ* data, there appears to be more of an east-west rather than north-south divide (Rodier et al., 2021).

Modelled uptake rates of both NH_4 and NO_x were highest at L1 and lowest at L4 (**Fig. 6B**). This may be due to different residence times across the lagoon which are highest near L1 (Dumas et al., 2012). In addition, L1 is in a particularly shallow part of the lagoon, in close proximity to a local village (which may add anthropogenic inputs) and to high-density pearl farms (Andréfouët et al., 2012). In contrast, L4 has the lowest residence time as it is near the pass and thus exposed to more oligotrophic oceanic water (Dumas et al., 2012). These spatial differences are also visible in the *in situ* data (Rodier et al., 2021). Nevertheless, since the model is 0D, the inflow of oceanic water through the pass is not accounted for and the above explanations cannot be used to explain the differences observed in the model results which must therefore be due to differences in the initial conditions.

Moreover, in the reference simulation, NH_4 uptake by nano- represented less than 50 % of the total, except at L1 and L8. The same results were found *in situ* by Rodier et al. (2021) for L1, where nano- uptake reached 57% of the total, but not at L8. This may be again due to the fact that L1 is located near high-density pearl farms (Andréfouët et al., 2012), hence nano-, which is more grazed by oysters, may have adapted to the higher grazing pressure by increasing their NH_4 uptake rates. L8 is not well represented by the model which may also be due to its particular location at the confluence of the two main circulation cells (Dumas et al., 2012). This station is thus influenced by both, oceanic water entering through the pass and nutrient rich water coming from the SW part of the lagoon. As the model does not account for any horizontal transport, it cannot represent this phenomenon correctly. The present results

thus merely reflect of our choice of initial conditions. At all stations, NO_x uptake was lower than NH_4 uptake, in both *in situ* data and the model results. In the model, L1 showed the highest NO_x uptake while *in situ* the uptake was highest at L0. Our choice of the initial phytoplankton biomass at L0 may have been too low compared to *in situ* data. Concerning the ratio of NO_x uptake between pico- and nano-, measurements showed clear spatial differences across the lagoon, with 37 % of total NO_x uptake by nano- at L1 and > 50 % in the other parts of the lagoon**.** In the model, on the contrary, the NOx uptake due to picophytoplankton is elsewhere greater than those due to nanophytoplankton at all the stations.

4.3. Determining the sources of N input

Grazing on phytoplankton may vary depending on the type of predator. As expected, in the model, a higher grazing rate led to a decrease in phytoplankton biomass and an increase of nutrient concentrations. However, pico- was sensitive to changes in grazing on nano-, while nano- was not sensitive to changes in grazing on pico-. In addition, while NH_4 seemed rather sensitive to changes in grazing it was relatively unaffected by other parameter changes (simulations S2-4). In contrast, NOx was less affected by changes in grazing pressure and more sensitive to changes in the other parameters. In the grazing simulations (S1.x), the nano-biomass values were closer to the *in situ* ranges which confirms that nano- would be preferentially grazed by oysters and other higher predators. Moreover, modeled NH_4 concentrations in the grazing and benthic fluxes simulations (S2) were closer to *in situ* values. The model thus seems to confirm that part of the remineralization described in Ahe by Lacoste and Gaertner-Mazouni (2016). Gaertner-Mazouni et al. (2012) concluded that benthic fluxes may contribute to meet phytoplankton nitrogen requirements near oyster farms. Grenz et al. (this issue) also observed noticeable exchanges between the sediment and water column near farms. The S2 simulation seems to confirm that remineralization occurs in sediments and represents about 4 % of the phytoplankton NH_4 uptake, which is consistent with the percentage measured by Rodier et al. (2021).

Except at L1 station where initial NO_x concentrations were high, the modeled NO_x concentrations in S0 were lower than *in situ* data in. To increase these low concentrations, we tested different hypotheses. First, Charpy-Roubaud et al. (2001) showed that atmospheric N_2 fixation was a potential source of nitrogen input to lagoons. By adding this source, we could increase the NO_x concentration in the model. N_2 fixation may enrich the water column with NH_4 after remineralization. Subsequent nitrification can then transform ammonium to nitrates. This nitrification was boosted in the model, which is why, by implementing N_2 fixation, the

model showed an increase in NO_x. While data on N_2 fixation was available for Tikehau Atoll there were no data for Ahe. The high values of NO_x measured in the rain water and ground water lens could be due to human activities on the *motu* or to the local avifauna (Otero et al., 2018). The improvement representation of NO_x concentration in simulations S3 and S4 confirms that additional NO_x inputs are indeed quite likely. Other hypotheses can also explain this high NO_x concentrations, namely upwelling generated by an overturning circulation cell in the north-eastern part of the lagoon (Dumas et al., 2012).

4.4. Conclusions and future work

While many hypotheses have been made to explain the nitrogen cycle and specifically the origin of nitrogen in Polynesian atolls, it is still not completely understood. Modelling provides a useful tool to quickly test these hypotheses. In this study, we used the new ECO3M-Atoll model to run a set of simulations to test some of these hypotheses in the Ahe lagoon. Overall, the model results were is similar ranges than the *in situ* data. The simulations improved our understanding of the biogeochemical functioning of Ahe Atoll. More specifically, we could confirm that nano- are grazed by oysters and higher predators (Dupuy et al., 2009). Simulations to test the impacts of grazing and benthic fluxes showed the ability of the model to represent the impact of remineralization by the grazing in water column and the sediment. Finally, nitrogen fixation and NO_x inputs allowed to increase the low NO_x concentrations.

One of the limitations in our approach was that we set the same light and temperature conditions at all five stations. We did this because the sensitivity analysis did not show any significant variability in phytoplankton biomass for the range of PAR and temperature values observed during the AHE2017 field campaign. Nevertheless, *in situ* data showed small spatial variabilities in temperature and phytoplankton community composition between the SW and the other areas of Ahe lagoon. This could not be reproduced by our model. However, the observed variation in phytoplankton communities may be caused by various factors such as the presence of other organisms, nutrient conditions, pearl farms, anthropic inputs, etc. Moreover, the d_C and d_N parameters were much more sensitive than in the ECO3M-Lagoon configuration on which our ECO3M-Atoll model is based. This may be due to respiration being constant and the fact that we used two instead of one phytoplankton compartment. In the future, respiration could be controlled via a similar quota-based function that already controls nutrient uptake and growth.

The model was run in 0D, which means that the forcing was constant and the hydrodynamics (circulation, stratification, vertical mixing, etc.) were not represented. In the future, ECO3M-Atoll will be coupled with a hydrodynamic model (MARS3D) will introduce some more realism and variability to the modelled processes to facilitate a more in-depth understanding of how the hydrodynamics and different temperatures and irradiances may influence the biogeochemistry at Ahe Atoll. Moreover, by upgrading the model to 3D, the forcing (grazing by oysters, benthic fluxes, anthropogenic inputs, N fixation) can vary spatially and as a function of depth. Finally, the coupled model should be able to provide information regarding the trophic forcing to the oyster dynamic energy budget (DEB) model by Thomas et al. (2012) (see also Sangare et al., 2019). This set of coupled models will help to investigate the influence of biogeochemistry on the life cycle of pearl oysters and on the farming activity.

To conclude, this study presented the ECO3M-Atoll model, a new biogeochemical model specifically configured for Ahe Atoll to study the nitrogen cycle and biogeochemical ecosystem functional in a pearl farming atoll. A better understanding of the local nitrogen cycle is pivotal to understand local phytoplankton dynamics, the principal food item of pearl oysters in deep and semi-closed atolls. Future implementations of the physical-biogeochemical-DEB coupled model will contribute to the improved management of pearl farms, not only at Ahe but also at other pearl farming atolls of the Tuamotu Archipelago that show a similar geomorphology to Ahe Atoll.

Acknowledgments

This study was funded by the ANR-16-CE32-0004 MANA (Management of Atolls) project. The authors acknowledge the staff of the "Cluster de calcul intensif HPC" Platform of the OSU Institut Pythéas (Aix-Marseille Université, INSU-CNRS) for providing the computing facilities. We gratefully acknowledge Julien Lecubin and Christophe Yohia from the Service Informatique de OSU Institut Pythéas (SIP) for their technical assistance. Finally, we are also grateful to XpertScientific for English corrections and the two anonymous reviewers for their helpful, their advice and valuable comments which have greatly contributed to improving the manuscript.

References

Andréfouët, S., Charpy, L., Lo-Yat, A., Lo, C., 2012. Recent research for pearl oyster aquaculture management in French Polynesia. Marine Pollution Bulletin 65, 407–414. https://doi.org/10.1016/j.marpolbul.2012.06.021

Baklouti, M., Diaz, F., Pinazo, C., Faure, V., Quéguiner, B., 2006. Investigation of mechanistic formulations depicting phytoplankton dynamics for models of marine pelagic ecosystems and description of a new model. Progress in Oceanography 71, 1–33. https://doi.org/10.1016/j.pocean.2006.05.002

Baklouti, Melika, Faure, V., Pawlowski, L., Sciandra, A., 2006. Investigation and sensitivity analysis of a mechanistic phytoplankton model implemented in a new modular numerical tool (Eco3M) dedicated to biogeochemical modelling. Progress in Oceanography 71, 34–58. https://doi.org/10.1016/j.pocean.2006.05.003

Binet, D., Le Borgne, R., 1996. The coastal station of Nouméa: ten years of observations about the hydrology and pelagos of the south-west lagoon of New- Caledonia. Archives Sciences de la Mer Biologie Marine, Editions IRD, Nouméa 37.

Bouvy, M., Dupuy, C., Pagano, M., Barani, A., Charpy, L., 2012. Do human activities affect the picoplankton structure of the Ahe atoll lagoon (Tuamotu Archipelago, French Polynesia)? Marine Pollution Bulletin 65, 516–524. https://doi.org/10.1016/j.marpolbul.2012.01.008

Chapelle, A., Ménesguen, A., Deslous-Paoli, J.-M., Souchu, P., Mazouni, N., Vaquer, A., Millet, B., 2000. Modelling nitrogen, primary production and oxygen in a Mediterranean lagoon. Impact of oysters farming and inputs from the watershed. Ecological Modelling 127, 161–181. https://doi.org/10.1016/S0304-3800(99)00206-9

Charpy, L., Charpy-Roubaud, C.J., 1990. Trophic Structure and Productivity of the Lagoonal Communities of Tikehau Atoll (Tuamotu Archipelago, French-Polynesia). Hydrobiologia 207, 43–52.

Charpy, L., Rodier, M., Fournier, J., Langlade, M.-J., Gaertner-Mazouni, N., 2012. Physical and chemical control of the phytoplankton of Ahe lagoon, French Polynesia. Marine Pollution Bulletin 65, 471–477. https://doi.org/10.1016/j.marpolbul.2011.12.026

Charpy-Roubaud, C., Charpy, C., Larkum, A.W.D., 2001. Atmospheric dinitrogen fixation by benthic communities of Tikehau Lagoon (Tuamotu Archipelago, French Polynesia) and its contribution to benthic primary production. Marine Biology 139, 991–998. https://doi.org/10.1007/s002270100636

Cugier, P., Struski, C., Blanchard, M., Mazurié, J., Pouvreau, S., Olivier, F., Trigui, J.R., Thiébaut, E., 2010. Assessing the role of benthic filter feeders on phytoplankton production in a shellfish farming site: Mont Saint Michel Bay, France. Journal of Marine Systems 82, 21–34. https://doi.org/10.1016/j.jmarsys.2010.02.013

Dowd, M., 2005. A bio-physical coastal ecosystem model for assessing environmental effects of marine bivalve aquaculture. Ecological Modelling 183, 323–346. https://doi.org/10.1016/j.ecolmodel.2004.08.018

Dufour, P., Andrefouet, S., Charpy, L., Garcia, N., 2001. Atoll morphometry controls lagoon nutrient regime. Limnol. Oceanogr. 46, 456–461.

Dumas, F., Le Gendre, R., Thomas, Y., Andréfouët, S., 2012. Tidal flushing and wind driven circulation of Ahe atoll lagoon (Tuamotu Archipelago, French Polynesia) from in situ observations and numerical modelling. Marine Pollution Bulletin 65, 425–440. https://doi.org/10.1016/j.marpolbul.2012.05.041

Dupuy, C., Bouvy, M., Charpy, L., Fournier, J., Pagano, M., Durieux, B., Thomas, Y., Michotey, V., Champalbert, G., Boeuf, D., Guasco, S., Lo-Yat, A., 2009. Planktonic compartment of Ahe Atoll (Tuamotu Archipelago, French Polynesia): potential preys for pearl oyster Pinctada margaritifera 6.

Dutheil, C., Andrefouët, S., Jullien, S., Le Gendre, R., Aucan, J., Menkes, C., 2020. Characterization of south central Pacific Ocean wind regimes in present and future climate for pearl farming application. Marine Pollution Bulletin 160, 111584. https://doi.org/10.1016/j.marpolbul.2020.111584

Eppley, R.W., 1972. Temperature and phytoplankton growth in the sea. Fishery Bulletin 70, 1063–1085.

Everett, J.D., Baird, M.E., Suthers, I.M., 2007. Nutrient and plankton dynamics in an intermittently closed/open lagoon, Smiths Lake, south-eastern Australia: An ecological model. Estuarine, Coastal and Shelf Science 72, 690–702. https://doi.org/10.1016/j.ecss.2006.12.001

Faure, V., Pinazo, C., Torréton, J.-P., Douillet, P., 2010a. Modelling the spatial and temporal variability of the SW lagoon of New Caledonia II: Realistic 3D simulations compared with in situ data. Marine Pollution Bulletin 61, 480–502. https://doi.org/10.1016/j.marpolbul.2010.06.040

Faure, V., Pinazo, C., Torréton, J.-P., Douillet, P., 2006. Relevance of various formulations of phytoplankton chlorophyll a:carbon ratio in a 3D marine ecosystem model. Comptes Rendus Biologies 329, 813–822. https://doi.org/10.1016/j.crvi.2006.07.006

Faure, V., Pinazo, C., Torréton, J.-P., Jacquet, S., 2010b. Modelling the spatial and temporal variability of the SW lagoon of New Caledonia I: A new biogeochemical model based on microbial loop recycling. Marine Pollution Bulletin 61, 465–479. https://doi.org/10.1016/j.marpolbul.2010.06.041

Fournier, J., Levesque, E., Pouvreau, S., Pennec, M.L., Moullac, G.L., 2012. Influence of plankton concentration on gametogenesis and spawning of the black lip pearl oyster Pinctada margaritifera in Ahe atoll lagoon (Tuamotu archipelago, French polynesia). Marine Pollution Bulletin 65, 463–470. https://doi.org/10.1016/j.marpolbul.2012.03.027

Fuchs, R., Dupouy, C., Douillet, P., Caillaud, M., Mangin, A., Pinazo, C., 2012. Modelling the impact of a La Niña event on a South West Pacific Lagoon. Marine Pollution Bulletin 64, 1596–1613. https://doi.org/10.1016/j.marpolbul.2012.05.016

Fuchs, R., Pinazo, C., Douillet, P., Fraysse, M., Grenz, C., Mangin, A., Dupouy, C., 2013. Modelling ocean–lagoon interaction during upwelling processes in the South West of New Caledonia. Estuarine, Coastal and Shelf Science 135, 5–17. https://doi.org/10.1016/j.ecss.2013.03.009

Fukuda, R., Ogawa, H., Nagata, T., Koike, I., 1998. Direct Determination of Carbon and Nitrogen Contents of Natural Bacterial Assemblages in Marine Environments. Appl. Environ. Microbiol. 64, 3352–3358. https://doi.org/10.1128/AEM.64.9.3352-3358.1998

Gaertner-Mazouni, N., Lacoste, E., Bodoy, A., Peacock, L., Rodier, M., Langlade, M.-J., Orempuller, J., Charpy, L., 2012. Nutrient fluxes between water column and sediments: Potential influence of the pearl oyster culture. Marine Pollution Bulletin 65, 500–505. https://doi.org/10.1016/j.marpolbul.2012.02.013

Geider, R.J., Maclntyre, H.L., Kana, T.M., 1998. A dynamic regulatory model of phytoplanktonic acclimation to light, nutrients, and temperature. Limnol. Oceanogr. 43, 679–694. https://doi.org/10.4319/lo.1998.43.4.0679

Gerber, R.P., Gerber, M.B., 1979. Ingestion of natural particulate organic matter and subsequent assimilation, respiration and growth by tropical lagoon zooplankton. Marine Biology 52, 33–43.

Grenz, C., Rodier, M., Seceh, C., Varillon, D., Haumani, G., Pinazo, C., 2021. Benthic Nutrients and oxygen fluxes at the water sediment interface in a pearl farming atoll lagoon (Ahe, Tuamotu, French Polynesia), submitted.

Harmon, R., Challenor, P., 1997. A Markov chain Monte Carlo method for estimation and assimilation into models. Ecological Modelling 101, 41–59. https://doi.org/10.1016/S0304-3800(97)01947-9

Hochard, S., Pinazo, C., Grenz, C., Evans, J.L.B., Pringault, O., 2010. Impact of microphytobenthos on the sediment biogeochemical cycles: A modeling approach. Ecological Modelling 221, 1687–1701. https://doi.org/10.1016/j.ecolmodel.2010.04.002

Lacoste, É., Gaertner-Mazouni, N., 2016. Nutrient regeneration in the water column and at the sediment–water interface in pearl oyster culture (Pinctada margaritifera) in a deep atoll lagoon (Ahe, French Polynesia). Estuarine, Coastal and Shelf Science 182, 304–309. https://doi.org/10.1016/j.ecss.2016.01.037

Lazure, P., Dumas, F., 2008. An external–internal mode coupling for a 3D hydrodynamical model for applications at regional scale (MARS). Advances in Water Resources 31, 233–250. https://doi.org/10.1016/j.advwatres.2007.06.010

Le Borgne, R., Blanchot, J., Charpy, L., 1989. Zooplankton of tikehau atoll (Tuamotu archipelago) and its relationship to particulate matter. Marine Biology 102, 341–353. https://doi.org/10.1007/BF00428486

Le Borgne, R., Roger, C., 1983. Caractéristiques de la composition et de la physiologie des peuplements hauturiers de zooplancton et micronecton du Golfe de Guinée; Main features of the composition and physiology of open-ocean zooplankton and micronekton populations in the Gulf of Guinea. Océanogr. trop 18, 381–418.

Leblanc, K., Quéguiner, B., Diaz, F., Cornet, V., Michel-Rodriguez, M., Durrieu de Madron, X., Bowler, C., Malviya, S., Thyssen, M., Grégori, G., Rembauville, M., Grosso, O., Poulain, J., de Vargas, C., Pujo-Pay, M., Conan, P., 2018. Nanoplanktonic diatoms are globally overlooked but play a role in spring blooms and carbon export. Nat Commun 9, 953. https://doi.org/10.1038/s41467-018-03376-9

Lefebvre, S., Claquin, P., Orvain, F., Véron, B., Charpy, L., 2012. Spatial and temporal dynamics of size-structured photosynthetic parameters (PAM) and primary production (13C) of pico- and nano-phytoplankton in an atoll lagoon. Marine Pollution Bulletin 65, 478–489. https://doi.org/10.1016/j.marpolbul.2012.04.011

Lorenzen, C.J., 1972. Extinction of Light in the Ocean by Phytoplankton. ICES Journal of Marine Science 34, 262–267. https://doi.org/10.1093/icesjms/34.2.262

Maréchal, D., 2004. Cranfield University at Silsoe Institute of Water and Environment. Cranfield University.

Marinov, D., Galbiati, L., Giordani, G., Viaroli, P., Norro, A., Bencivelli, S., Zaldívar, J.-M., 2007. An integrated modelling approach for the management of clam farming in coastal lagoons. Aquaculture 269, 306–320. https://doi.org/10.1016/j.aquaculture.2007.04.071

Mongin, M., Baird, M., 2014. The interacting effects of photosynthesis, calcification and water circulation on carbon chemistry variability on a coral reef flat: A modelling study. Ecological Modelling 284, 19–34. https://doi.org/10.1016/j.ecolmodel.2014.04.004

Niquil, N., Jackson, G., Legendre, L., Delesalle, B., 1998. Inverse model analysis of the planktonic food web of Takapoto Atoll (French Polynesia). Mar. Ecol. Prog. Ser. 165, 17–29. https://doi.org/10.3354/meps165017

Otero, X.L., De La Peña-Lastra, S., Pérez-Alberti, A., Ferreira, T.O., Huerta-Diaz, M.A., 2018. Seabird colonies as important global drivers in the nitrogen and phosphorus cycles. Nat Commun 9, 246. https://doi.org/10.1038/s41467-017-02446-8

Pagano, M., Rodier, M., Guillaumot, C., Thomas, Y., Henry, K., Andréfouët, S., 2017. Ocean-lagoon water and plankton exchanges in a semi-closed pearl farming atoll

lagoon (Ahe, Tuamotu archipelago, French Polynesia). Estuarine, Coastal and Shelf Science 191, 60–73. https://doi.org/10.1016/j.ecss.2017.04.017

Pagano, M., Sagarra, P.-B., Champalbert, G., Bouvy, M., Dupuy, C., Thomas, Y., Charpy, L., 2012. Metazooplankton communities in the Ahe atoll lagoon (Tuamotu Archipelago, French Polynesia): Spatiotemporal variations and trophic relationships. Marine Pollution Bulletin 65, 538–548. https://doi.org/10.1016/j.marpolbul.2012.01.025

Pinazo, C., Bujan, S., Douillet, P., Fichez, R., Grenz, C., Maurin, A., 2004. Impact of wind and freshwater inputs on phytoplankton biomass in the coral reef lagoon of New Caledonia during the summer cyclonic period: a coupled three-dimensional biogeochemical modeling approach. Coral Reefs 23. https://doi.org/10.1007/s00338-004-0378-x

Pouvreau, S., Tiapari, J., Gangnery, A., Lagarde, F., Garnier, M., Teissier, H., Haumani, G., Buestel, D., Bodoy, A., spouvrea@ifremer, fr, 2000. Growth of the black-lip pearl oyster, Pinctada margaritifera, in suspended culture under hydrobiological conditions of Takapoto lagoon (French Polynesia). Aquaculture 184, 133–154.

Projet 9ème FED Professionnalisation et perennisation de la perliculture, 2010. Résultats des activités scientifiques FED - Recueil de fiches thématiques (Livret fiche). Service de la perliculture, Papeete, Tahiti.

Redfield, A., Ketchum, B., Richards, F., others, 1963. The influence of organisms on the composition of seawater. The sea 2, 26–77.

Rodier, M., Pinazo, C., Seceh, C., Varillon, D., 2021. Pelagic stocks and fluxes of carbon and nitrogen in a pearl farming atoll (Ahe, Fren Polynesia). Marine Pollution Bulletin In review.

Rougerie, F., Fagerstrom, J.A., Andrie, C., 1992. Geothermal Endoupwelling - A Solution to the Reef Nutrient Paradox. Continental Shelf Research 12, 785–798.

Sangare, N., Lo-Yat, A., Le Moullac, G., Pecquerie, L., Thomas, Y., Beliaeff, B., Andréfouët, S., 2019. Estimation of physical and physiological performances of blacklip pearl oyster larvae in view of DEB modeling and recruitment assessment. Journal of Experimental Marine Biology and Ecology 512, 42–50. https://doi.org/10.1016/j.jembe.2018.12.008

Shelford, E.J., Middelboe, M., Møller, E.F., Suttle, C.A., 2012. Aquatic Microbial Ecology 66:41. Aquat Microb Ecol 6.

Smith, C.L., Tett, P., 2000. A depth-resolving numerical model of physically forced microbiology at the European shelf edge. Journal of Marine Systems 26, 1–36. https://doi.org/10.1016/S0924-7963(00)00010-5

Tett, P., 1990. A Three Layer Vertical and Microbiological Processes Model for Shelf Seas (No. 14). Proudman Oceanographic Laboratory, Birkenhead.

Tett, P., 1987. Modelling the growth and distribution of marine microplankton., in: Symposia of the Society for General Microbiology(Cambridge)[SYMP. SOC. GEN. MICROBIOL.(CAMB.).]. 1987.

Thingstad, T., 1987. Utilization of N, P, and organic C by heterotrophic bacteria. I. Outline of a chemostat theory with a consistent concept of "maintenance" metabolism. Mar. Ecol. Prog. Ser. 35, 99–109. https://doi.org/10.3354/meps035099

Thomas, Y., Dumas, F., Andréfouët, S., 2016. Larval connectivity of pearl oyster through biophysical modelling; evidence of food limitation and broodstock effect. Estuarine, Coastal and Shelf Science 182, 283–293. https://doi.org/10.1016/j.ecss.2016.03.010

Thomas, Y., Garen, P., Courties, C., Charpy, L., 2010. Spatial and temporal variability of the pico- and nanophytoplankton and bacterioplankton in a deep Polynesian atoll lagoon. Aquatic Microbial Ecology 59, 89–101. https://doi.org/10.3354/ame01384

Thomas, Y., Le Gendre, R., Garen, P., Dumas, F., Andréfouët, S., 2012. Bivalve larvae transport and connectivity within the Ahe atoll lagoon (Tuamotu Archipelago), with application to pearl oyster aquaculture management. Marine Pollution Bulletin 65, 441–452. https://doi.org/10.1016/j.marpolbul.2011.12.027

Weise, A.M., Cromey, C.J., Callier, M.D., Archambault, P., Chamberlain, J., McKindsey, C.W., 2009. Shellfish-DEPOMOD: Modelling the biodeposition from suspended shellfish aquaculture and assessing benthic effects. Aquaculture 288, 239–253. https://doi.org/10.1016/j.aquaculture.2008.12.001

Wild, C., Huettel, M., Klueter, A., Kremb, S.G., Rasheed, M.Y.M., Jørgensen, B.B., 2004. Coral mucus functions as an energy carrier and particle trap in the reef ecosystem. Nature 428, 66–70. https://doi.org/10.1038/nature02344

Willmott, C.J., 1982. Some Comments on the Evaluation of Model Performance. Bulletin American Meteorological Society 63, 5.